Seventh International Symposium on Marine Propulsors
SMP2022, Wuxi, China, October 17-21, 2022

Predicting the higher-order harmonics of propeller-induced hull-pressure fluctuations by tip-vortex cavitation

Johan Bosschers

Maritime Research Institute Netherlands (MARIN), Wageningen, The Netherlands

ABSTRACT

Cavitating propellers generate pressure fluctuations on the hull of the ship and emit underwater sound. These pressure fluctuations are usually analysed in the frequency domain with the spectrum composed of tonals at harmonics of the blade passage frequency and a broadband part. The two are often analysed separately through the amplitudes of the tonals and through the power density or power spectrum of the broadband part. The present paper discusses an analytical formulation that shows how the two are related through the variability of the pressure signal between blade passages. The formulation is also used to predict the tonals from the broadband part of the spectrum for which an semi-empirical model for tip-vortex cavitation is available.

Keywords

Propellers, hull-pressure fluctuations, tip-vortex cavitation, tonals, broadband.

1 INTRODUCTION

Cavitating propellers may generate noise and vibration hindrance for crew and passengers on-board ships (Carlton, 2007). Often, it is the spectrum of the pressure fluctuations on the hull above the propeller that are analysed to evaluate the hull-excitation force of the cavitating propeller. The frequency range typically varies from the blade-passage frequency (BPF) up to 200 Hz when the vibration excitation force is considered, but analysis up to higher frequencies are nowadays performed as well. Propeller cavitation is also an important contributor to the underwater radiated noise (URN) of ships. The URN of ships was traditionally of importance for naval vessels and fishery research vessels only, but is nowadays also of importance for merchant vessels due to impact of shipping noise on marine life (Duarte et al, 2021; Cruz et al, 2021).

At low frequencies, the propeller-induced pressure spectrum is composed of tonal components at harmonics of the blade passage frequency and of a broadband part. Tonals are also present for a non-cavitating propeller, and are due to the thickness and loading of the propeller blade (see e.g. Breslin, 1970, and Lafeber *et al*, 2009). This tonal is very pronounced at the BPF but its amplitude decreases rapidly at the 2nd and higher harmonics of the BPF. The amplitudes of the higher harmonics relative to the BPF value depend on the number of blades and on the propeller-hull clearance. The tonals due to the cavitating propeller are discussed by e.g. van der Kooij (1979), Friesch (1998), van Wijngaarden (2011), and Johannsen et al. (2012). One of the first publications on broadband content of hull-pressure fluctuations is by Brubakk and Smogeli (1988), discussing vibration issues on a cruisevessel which were related to the cavitating tip vortex. Measurements of broadband spectra of hull-pressures on twin-screw vessels were presented by among others Fréchou et al (2000), Hämäläinen et al. (2005) and Bosschers (2009). The topic was also briefly addressed by the 23rd ITTC Specialist Committee on Cavitation Induced Pressures (2002).

Various models have been proposed in literature to predict the low-frequency part of propeller-induced pressure spectrum, either for hull-pressure fluctuations or for URN. Semi-empirical models, making use of results obtained by boundary element method, to predict the broadband part have been proposed by among others Raestad (1996), Bosschers (2018b) and Miglianti et al. (2019). Berger et al. (2018) uses its model to predict the broadband part and the tonals at higher harmonics of the BPF. Examples of RANS predictions are provided by e.g. Vaz et al (2015) and Ge et al (2020), whereas results of scale resolving simulations are presented by Li et al (2016) and Lidtke et al (2022).

The present paper discusses a method to include the prediction of tonals in an existing method to predict the broadband part that makes use of a boundary element method (Bosschers, 2018b). The method is based on an analytically derived formulation that describes the relation between the two as a function of the variation in the pressure signal between blade passages. Next, it is shown how this variation can be quantified from model-scale data as well as full-scale data. Analysis of multiple test-cases, all twin-screw vessels, provided a typical value for the variation which is then used as an additional empirical input parameter for the model to predict the tonals from the broadband content.

2 ANALYTICAL FORMULATION

2.1 Derivation

The derivation for the analytical formulation to describe the effect of the variability of a periodic signal is based on MacFarlane (1949), but differs by considering the effect of variability in amplitude and time of arrival of the periodic signal simultaneously instead of treating them separately. The details of the derivation are given in Bosschers (2018a).

Consider the rms amplitude density spectrum $G(\omega)$ of a single pulse of unit amplitude. The spectrum of the same pulse occurring at a later time t is then given by

$$G(\omega)\exp(i\omega t) \tag{1}$$

Now assume that the pulse is emitted periodically with mean period *T*, but each pulse is emitted with a slightly varying amplitude a_n and time offset τ_n. The resulting spectrum for 2N periods then reads

$$S(\omega) = G(\omega) \sum_{n=-N}^{N} a_n \exp\left[i\omega\left(nT+\tau_n\right)\right] \tag{2}$$

and the corresponding power spectral density is given by

$$\begin{aligned} R_N(\omega) &= \frac{\|S(\omega)\|^2}{(2N+1)} \\ &= \|G(\omega)\|^2 \left\{ \frac{1}{2N+1} \left\| \sum_{-N}^{N} a_n \exp\left[i\omega\left(nT+\tau_n\right)\right] \right\|^2 \right\} \end{aligned} \tag{3}$$

It is now assumed that both amplitude and time variation can be described by a Gaussian distribution:

$$q(a_n) = \frac{1}{\sigma_a\sqrt{2\pi}} \exp\left[-\left(a_n-\bar{a}\right)^2 / 2\sigma_a^2\right] \tag{4}$$

$$q(\tau_n) = \frac{1}{\sigma_\tau\sqrt{2\pi}} \exp\left(-\tau_n^2 / 2\sigma_\tau^2\right) \tag{5}$$

with $\bar{a}$ the mean amplitude, and σ_a and σ_τ the standard deviation of the amplitude and time period, respectively.

Equation (3) is evaluated by expanding the exponential function into sine and cosine functions, and by considering that the norm of a signal is computed by taking the norm of the mean and the norm of the standard deviation. After lengthy derivation, the formulation for the power spectral density reads

$$R(\omega) = \left\{ \sigma_a^2 + \bar{a}^2 \left[1 - \left\{ 1 - \omega_r \Delta_T(\omega) \right\} e^{-\omega^2\sigma_\tau^2} \right] \right\} \|G(\omega)\|^2 \tag{6}$$

Parameter $\omega_r = 2\pi/T$ is the repetition (angular) frequency, and $\Delta_T(\omega)$ is the Dirac comb for mean time period T, or frequency ω_r. The Dirac comb is related to the Dirac delta function $\delta(\omega)$ through

$$\Delta_T(\omega) = \sum_{m=-\infty}^{\infty} \delta\left(\omega - \frac{2\pi m}{T}\right) \tag{7}$$

In absence of any variation in amplitude and arrival time, the power spectral density is given by

$$R\left(\omega, \sigma_{a,\tau}=0\right) = \bar{a}^2\, \omega_r \Delta_T(\omega) \left\|G(\omega)\right\|^2 \tag{8}$$

Hence, the spectrum contains of tonals at harmonics of the repetition frequency only. However, as $\delta(0)\to\infty$, the amplitude of these tonals are formally not defined and a power spectrum *P* should be considered rather than the power spectral density:

$$\begin{aligned} P(\omega_c) &= \int_{\omega_c-\frac{1}{2}\Delta\omega}^{\omega_c+\frac{1}{2}\Delta\omega} R\left(\omega, \sigma_{a,\tau}=0\right) d\omega \\ &= \bar{a}^2\, \omega_r \sum_{m=1}^{\infty} \left\|G(m\omega_r)\right\|^2 \end{aligned} \tag{9}$$

where use has been made of

$$\int_{\left(m-\frac{1}{2}\right)\omega_r}^{\left(m+\frac{1}{2}\right)\omega_r} \Delta_T\left(m\,\omega_r\right) d\omega = 1 \tag{10}$$

The rms amplitudes of the tonals at harmonics of ω_r of $G(\omega)$ are scaled with a frequency bandwidth ω_r such that total power is conserved.

Equation (6) shows that the variation in amplitude and arrival time lead to broadband content in the spectrum. The broadband content due to amplitude variation is a frequency-independent fraction of the reference spectrum, provided σ_a is independent of frequency. However, the broadband fraction due to time variation does scale with frequency due to term $\exp\left(-\omega^2\sigma_\tau^2\right)$. The variation in time of arrival can be interpreted from a spectral content point of view as a variation in phase angle, with the standard deviation in phase given by

$$\sigma_\theta(\omega) = \omega\sigma_\tau \tag{11}$$

From Eq. (6) it is also seen that the exponential increase in broadband content with frequency is accompanied by an exponential decrease of the amplitude of the tonals at harmonics of the repetition frequency.

2.2 Interpretation

The preceding formulation can be interpreted as the formulation for the periodic pressure pulses generated by the collapse of a cavity when the propeller blade leaves the wake peak. Hence the repetition frequency of the pulse is the blade passage frequency bpf ($\omega_r = 2\pi f_{bp}$), and we investigate the consequences of variations in cavity collapse between subsequent blade passages.

The effect of the amplitude and phase angle modulation is illustrated in Figure 1 and Figure 2, following Bark (1988). A stylised spectrum is sketched of a single blade passage together with the spectrum of a series of blade passages. The frequency is non-dimensionalized by the bpf. If the signal repeat perfectly there is no modulation and the spectrum consists of tonals at harmonics of the bpf. Random variations in amplitude alone between different blade passages lead to a small increase of the amplitudes of the tonals. However, the spectrum now also contains a broadband part of which the magnitude is proportional to the standard deviation of the amplitude variations. Random changes in time of arrival of the signal lead to random phase angle variations of which the magnitude increases

linearly with frequency as shown by Eq. (11). This random phase modulation decreases the amplitude of the tonals and redistributes the power over a broadband region. The spreading is most pronounced at higher frequencies and may cause the complete disappearance of the tonal.

It is remarked that the variation in emitted pressure by the cavity collapse is expected to be more complex than the presented variation in amplitude and time-of-arrival in the sense that the spectral shape may also vary somewhat. This aspect is further discussed in Section 3.2 through the analysis of experimental data. In general, one can conclude that the broadband part of the spectrum is caused by the variability of the pressure signal between subsequent blade passages. It is especially the variation in phase angle that affects the spectrum as it reduces the amplitude of the tonals and increases the broadband part.

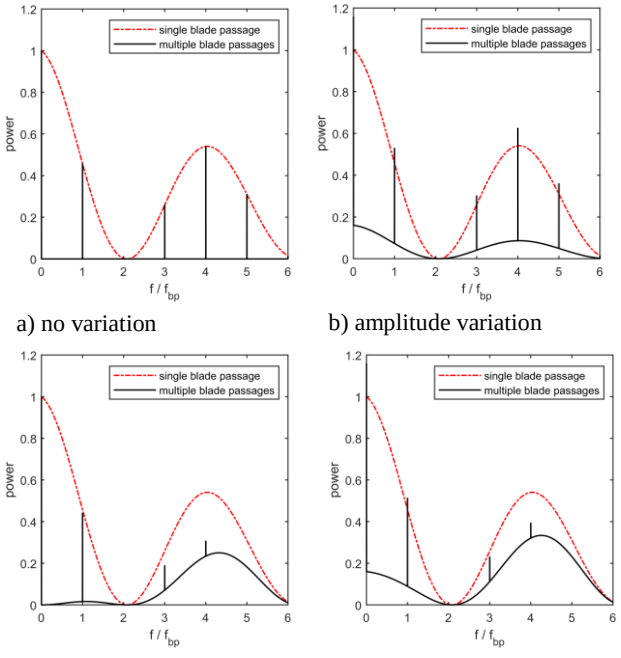

a) no variation b) amplitude variation

c) time variation d) amplitude and time variation

Figure 1: Effect of amplitude and arrival time variation on the power spectrum. Note that the spectrum of the single blade passage is a scaled power density spectrum.

3 ANALYSIS OF EXPERIMENTAL DATA

3.1 Analysis procedure

The variability between blade passages will now be investigated for both model-scale and full-scale experimental datasets. The goal is to find quantitative values for the amplitude and phase angle variations.

The hull-pressure signal has been analyzed by first dividing the time trace into 'shaft revolutions' with a shaft revolution defined by a constant number of samples that does not change in time. This number of samples, that is representative of the mean revolution rate of the shaft, was determined from a color-coded plot of the time trace with blade position and shaft revolution. The number of samples was defined as a real number if the data was time synchronized instead of shaft synchronized. Each shaft revolution was analyzed with an FFT which provided the amplitude and phase for each harmonic of the shaft-rate frequency. The data of all shaft revolutions was then used to compute the mean and the standard deviation. The procedure is straightforward for the amplitude variation, while for the variation in phase angle σ_θ use has been made of the theory of circular statistics (Fisher, 1993),

$$\sigma_\theta(\omega) = \sqrt{-2\ln\rho(\omega)} \qquad (12)$$

with ρ corresponding to the length of the mean resultant, computed from the phase angle θ_n of revolution number n at frequency ω,

$$\rho(\omega) = \sqrt{\left[\frac{1}{N}\sum_{n=1}^{N}\cos\theta_n(\omega)\right]^2 + \left[\frac{1}{N}\sum_{n=1}^{N}\sin\theta_n(\omega)\right]^2} \qquad (13)$$

with N the total number of shaft revolutions.

3.2 Results

Results of the analysis procedure described above are presented for two test-cases, both twin-screw vessels of which the cavitation pattern consists of mainly tip-vortex cavitation.

The first test-case was measured at model scale and the -data has been shaft synchronized. The time trace of the pressure signal plotted as function of blade position and revolution is presented with its analysis in Figure 2. The four blade passages for each shaft revolution can clearly be discerned. Analysis of the Fourier transforms for each revolution separately provides the presented values for the standard deviation for amplitude and phase. As the first harmonic of the BPF is for a significant part affected by the thickness and loading ('non-cavitating' contribution), the variability in amplitude is much smaller for this frequency than for other frequencies. Note that the frequency resolution of the spectrum corresponds to the shaft rate frequency. The variation in phase angle at harmonics of BPF shows indeed a linear increase with frequency, suggesting that it corresponds to a variation in time as used in Section 2. The maximum possible variation in phase angle corresponds to +/- 180 deg, hence the maximum value for the standard deviation is limited (and much smaller than 180 deg.). For this situation, the maximum value for the standard deviation is about 135 deg, excluding one outlier. For such high values of the standard deviation the variation is most likely no longer described by a Gaussian distribution but this has not been further investigated. The non-dimensional spectrum presented on the bottom shows (i) a 'reference' line (Ref), corresponding to the spectrum taken of the whole time trace, (ii) an 'amplitude' line (Ampl.) in which the spectrum is shown using the standard deviation at harmonics of the shaft rate frequency for the broadband part and the mean value for the harmonics of the blade

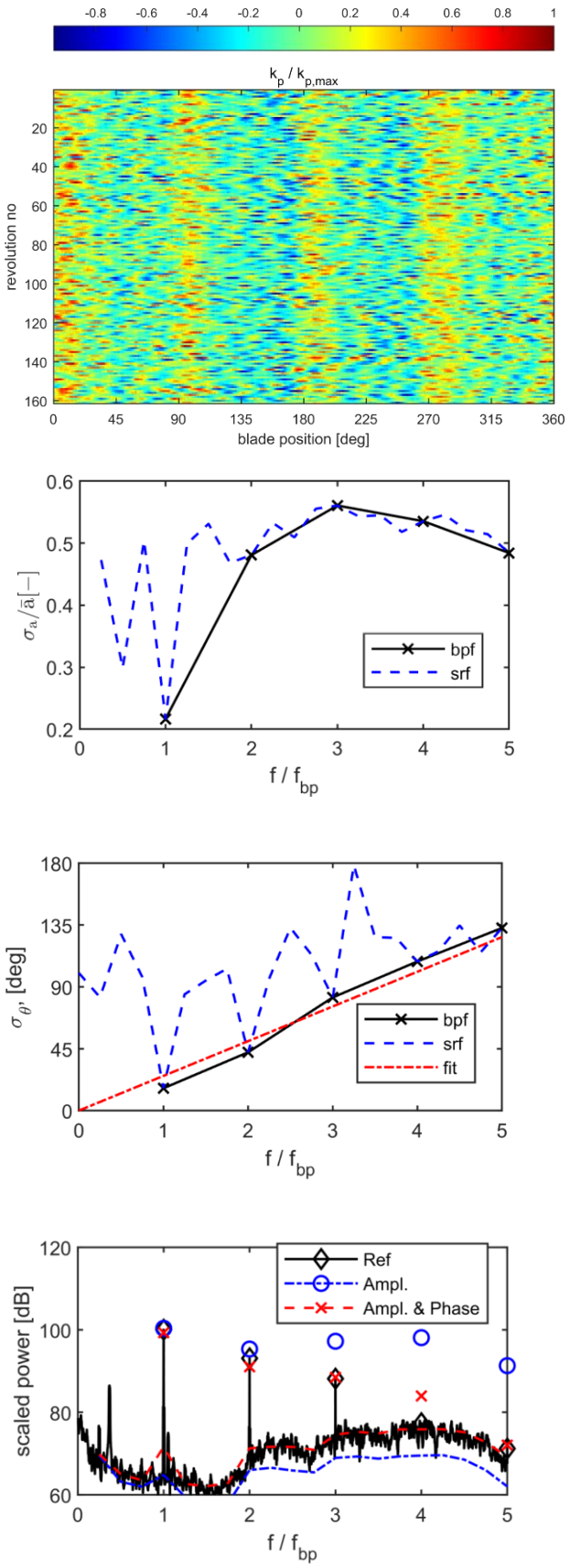

Figure 2: Analysis of amplitude and phase variation and its effect on the spectrum (model-scale test-case), showing from top to bottom the pressure time trace, the standard deviation of the amplitude, the standard deviation of the phase angle and the power spectrum for the various approaches.

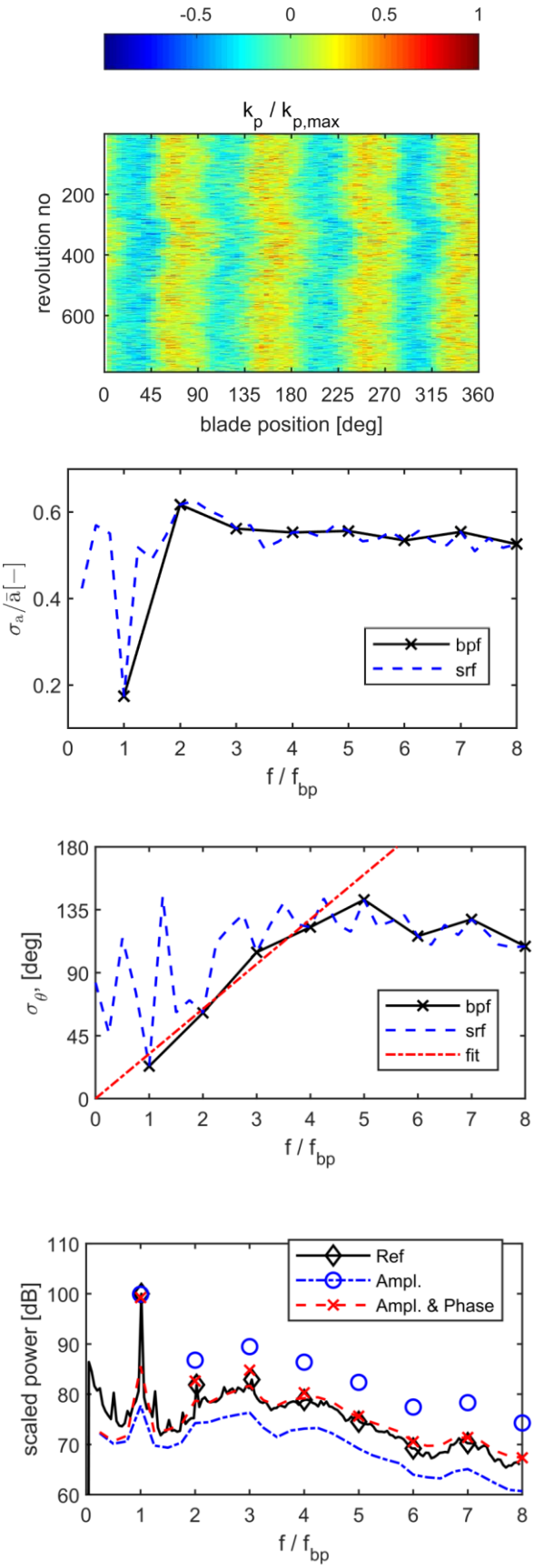

Figure 3: Analysis of amplitude and phase variation and its effect on the spectrum (full-scale test-case), showing from top to bottom the pressure time trace, the standard deviation of the amplitude, the standard deviation of the phase angle and the power spectrum for the various approaches.

passage frequency, and (iii) an 'amplitude and phase' line in which the 'amplitude' spectrum is corrected with the fitted line for the standard deviation of the phase angle for the blade-passage-frequencies. It is seen that the overall character of the 'reference' spectrum is well reconstructed from this approach.

The second test-case was measured at full scale and the data is not shaft synchronized. The time trace and its analysis are presented in

Figure **3**. The time trace shows a small variation in rpm, and that the propeller has four blades. The standard deviation of the amplitude is again small for the first BPF and has a value of about 0.5 for the higher harmonics. The variation of the standard deviation of the phase angle with harmonics of BPF shows again an almost linear variation with frequency up to the fourth harmonic after which the values remains more or less constant. With the fitted value for the standard deviation of the phase angle, the 'reference' spectrum is again well reconstructed.

It is remarked that to keep the graphs simple, the 'amplitude' spectrum only shows the mean values at harmonics of the BPF. The mean values at harmonics of the shaft-rate-frequency are not shown as due to the large values of the standard deviation of the phase they do not appear as tonals in the 'amplitude and phase' spectrum.

Nowadays, the hull-pressure measurements in sea trials are also shaft synchronized thereby eliminating the effect of variations in shaft rpm on the pressure spectrum. Analysis of this effect on a single screw vessel showed that the shaft synchronized data had a 20% smaller value for $\bar{\sigma}_\theta$ than the time-synchronized data. Of course, this effect strongly depends on sea state and maneuvers.

The cause of the variability between blade passages has not been investigated so far and this may vary from case to case and may be scale and facility dependent. Temporal variations in the ship wake field, including turbulence, are probably relevant, as well as variations in nuclei and gas content which usually show a stochastic distribution. In sea trials, also ship motions and the effect of rudder deflections can be relevant.

4 SEMI-EMPIRICAL PREDICTION MODEL

4.1 Introduction

The spectrum of hull-pressure fluctuations by tip-vortex cavitation can be predicted by the combination of the following methods:

1. The amplitude at bpf, dominated by the contributions of blade thickness and blade loading, predicted by the BEM *PROCAL* (Vaz and Bosschers, 2006) in combination with the acoustic BEM *EXCALIBUR (*Bosschers et al. 2008; van Wijngaarden, 2018*).*
2. The broadband part of the spectrum due to the cavitating tip-vortex is predicted by the semi-empirical ETV-method (Bosschers, 2018b).
3. The amplitudes at the harmonics of the bpf can now be predicted from the broadband part using the formulations derived in Section 2. Use is made of empirical values that describe the variation between blade passages obtained from the procedure described in Section 3. The formulations to predict the tonals from the broadband part are summarized below.

4.2 Predicting tonals from a broadband spectrum

It is assumed here that use can be made of an existing model for the broadband part of the spectrum. From the formulations derived in Section 2, this broadband spectrum can be formulated as

$$R_{broadband}(\omega) = \left\{ \frac{\sigma_a^2}{\bar{a}^2} + 1 - e^{-\omega^2 \sigma_\tau^2} \right\} \bar{a}^2 \left| G(\omega) \right|^2 \quad (14)$$

or when the circular frequency f is used instead of angular frequency,

$$R_{broadband}(f) = \left\{ \bar{\sigma}_a^2 + 1 - e^{-(f/f_{sr})^2 \bar{\sigma}_\theta^2} \right\} R_{ref}(f) \quad (15)$$

with $\bar{\sigma}_a = \sigma_a / a_n$, $\bar{\sigma}_\theta = \omega_{sr} \sigma_\tau$ in which subscript *sr* stands for shaft-rate frequency, and where a reference power density spectrum $R_{ref}(f) = \bar{a}^2 \left| G(f) \right|^2$ is introduced. Parameter $\bar{\sigma}_\theta$ is the standard deviation of the phase in radians per shaft-rate harmonic. The spectrum of the tonals at harmonic m of the BPF reads

$$R_{tonal}(m f_{bp}) = e^{-(m f_{bp}/f_{sr})^2 \bar{\sigma}_\theta^2} f_{bp} \Delta_T(m f_{bp}) R_{ref}(m f_{bp}) \quad (16)$$

The peak amplitude at this harmonic m of the BPF is computed by

$$A_{tonal}^2(m f_{bp}) = 2 \int_{(m-\frac{1}{2}) f_{bp}}^{(m+\frac{1}{2}) f_{bp}} R_{tonal}(m f_{bp})\, df \quad (17)$$

resulting into

$$A_{tonal}(m f_{bp}) = e^{-\frac{1}{2}(m f_{bp}/f_{sr})^2 \bar{\sigma}_\theta^2} \sqrt{2 f_{bp} R_{ref}(m f_{bp})} \quad (18)$$

A peak amplitude is preferred over the rms amplitude as harmonic analysis of propeller-induced hull-pressure fluctuations are traditionally expressed in peak amplitudes.

Hence, it is seen that from Eq. (15) for the semi-empirical model for the spectrum $R_{broadband}(f)$ of broadband noise and hull-pressure fluctuations the reference spectrum $R_{ref}(f)$ can be computed provided (empirical) values for $\bar{\sigma}_a$ and $\bar{\sigma}_\theta$ are known. The tonals at harmonics of the BPF can then be computed from Eq. (18) using the reference spectrum and $\bar{\sigma}_\theta$. An important assumption is that the values for $\bar{\sigma}_a$ and $\bar{\sigma}_\theta$ do not vary much between ships of the same ship type.

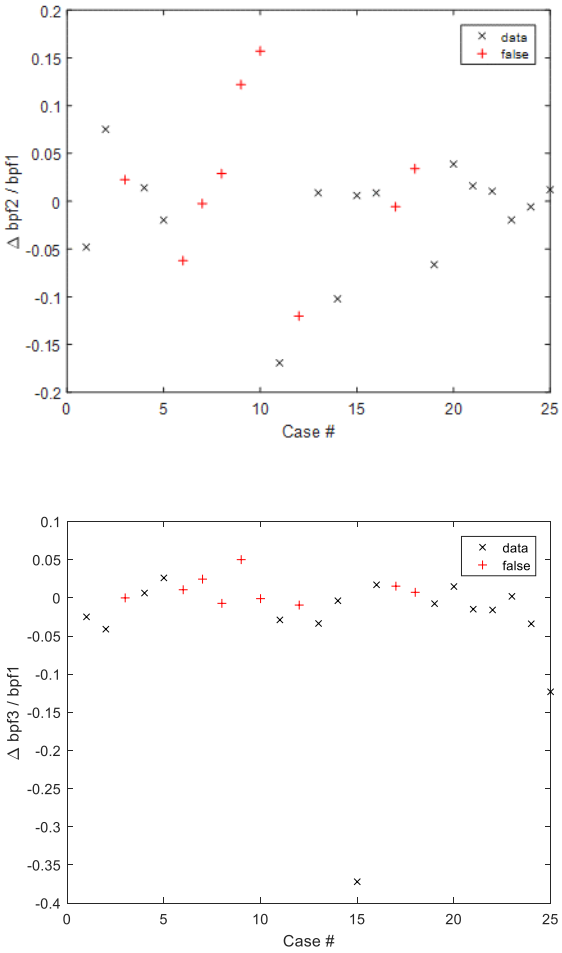

Figure 4: Error in the prediction of the amplitude at 2nd (top) and 3rd harmonic (bottom) of the blade passage frequency using the case-dependent variability for amplitude and phase.

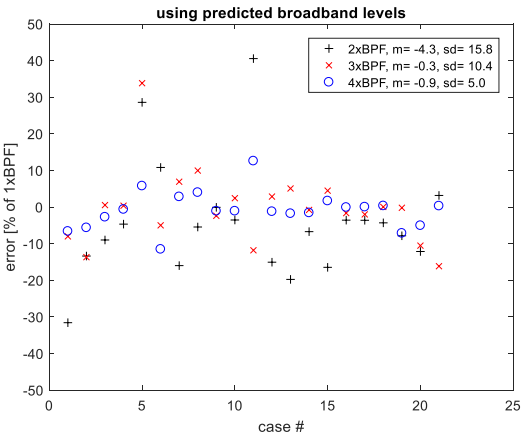

Figure 5: Prediction error for the harmonics using the broadband levels as predicted by the ETV-model and using the overall mean value for variability.

4.3 RESULTS

The analysis as shown in Figure 2 and

Figure **3** has been performed for 25 test-cases in total, all corresponding to twin-screw vessels. For each test-case the value for $\bar{\sigma}_\theta$ is computed by a linear fit through the values at the 2nd, 3rd, and 4th harmonic of the BPF, but excluding values that are larger than 90 degrees. The difference in amplitude at the harmonics of the BPF between the 'amplitude and phase' estimation and the 'reference' estimation are shown in Figure 4 for the second and the third BPF harmonic. For some of the datasets the variation of $\bar{\sigma}_\theta$ could not be described by a linear variation with frequency, these cases are denoted as 'false' in the figures. The judgement was made by visually inspecting each dataset. For these cases only the value for $\bar{\sigma}_\theta$ at the 2nd harmonic of the BPF was used. The amplitudes have been non-dimensionalized with the amplitude at the BPF, as for some cases the amplitude at the 2nd or 3rd harmonic of BPF was very small. Except for some outliers, the amplitudes can be reconstructed within 5% of the amplitude at BPF. From these test-cases, the average values for $\bar{\sigma}_a$ and $\bar{\sigma}_\theta$ have been determined, and they correspond to $\bar{\sigma}_a = 0.54$ and $\bar{\sigma}_\theta = 9.7\,\text{deg}$. The test-cases were then analyzed using the broadband hull-pressure prediction of the ETV-model, and the tonals were computed according to the procedure described in Section 4.2. It was then found that the mean prediction error could be improved by using $\bar{\sigma}_\theta = 9.0\,\text{deg}$. The results are shown in Figure 5, where it is seen that the 2nd harmonic is predicted with standard deviation of 16%, the 3rd harmonic with a standard deviation of 10%, and the 4th harmonic with a standard deviation of 5%, all relative to the amplitude of the first harmonic. The standard deviation of the relative prediction, hence relative to the amplitude of that specific harmonic, is 36% for the 2nd harmonic, 46% for the third harmonic and 87% of the fourth harmonic.

6 CONCLUDING REMARKS

A new methodology has been presented to predict the amplitudes of tonals of propeller-induced hull pressures at higher harmonics of the blade passage frequency. The methodology is based on an analytical formulation that describes the relation between the broadband part of the spectrum and the tonals, which is determined by the variability of the pressure signal between blade passages. The variability can be expressed as a variability in amplitude and phase of the spectral components. Multiple datasets, all for twin-screw vessels in which the cavitation pattern on the propeller was dominated by tip-vortex cavitation, were analyzed with respect to this variability. It was concluded that the relative variability in amplitude for frequencies above the blade passage frequency was more or less constant. The variability in phase at the harmonics of the blade passage frequency could for a large number of test-cases well be described by a linear variation with frequency. This suggests that an important mechanism for the variability in phase is indeed the variability in time-of-arrival of the pressure pulse due to the cavity collapse. This variability in time-of-arrival was a critical assumption in the derivation of the analytical formulation. Therefore, the

derived analytical formulation can both qualitatively and quantitatively explain the relation between tonals and broadband content of the hull-pressure spectrum.

It was found that by using two empirical parameters, one describing the variability in amplitude and one describing variability in phase, the amplitudes at the higher harmonics of the blade passage frequency can be obtained with a reasonable accuracy from a model that predicts the broadband part of the spectrum.

In the present paper the variability is only shown for twin-screw vessels of which the cavitation pattern is dominated by a tip-vortex cavity. Analysis for other ship types showed significant different values for the variability and this needs to be further investigated, together with the causes for the variability.

7 ACKNOWLEDGEMENTS

Part of the present analysis has been sponsored by the Cooperative Research Ships, Onboard working group (www.crships.org).

REFERENCES

Bark, G. (1988). 'On the mechanisms of propeller cavitation noise'. Ph.D. thesis, Chalmers University of Technology, Göteborg, Sweden.

Berger, S., Gosda, R., Scharf, M., Klose, R., Greitsch, L., and Abdel-Maksoud, M. (2016). 'Efficient numerical investigation of propeller cavitation phenomena causing higher-order hull pressure fluctuations'. In 31st Symposium on Naval Hydrodynamics, Monterey, California, USA.

Bosschers, J., Vaz, G., Starke, A.R., and van Wijngaarden, E. (2008). 'Computational analysis of propeller sheet cavitation and propeller-ship interaction'. In Proceedings of the RINA MARINE CFD Conference, Southampton, UK.

Bosschers, J. (2009). 'Investigation of hull pressure fluctuations generated by cavitating vortices'. First International Symposium on Marine Propulsors, smp'09, Trondheim, Norway.

Bosschers, J., (2018a). 'Propeller tip-vortex cavitation and its broadband noise'. PhD thesis, University of Twente, Enschede, the Netherlands.

Bosschers, J. (2018b). 'A semi-empirical prediction method for broadband hull pressure fluctuations and underwater radiated noise by propeller tip vortex cavitation'. Journal of Marine Science and Engineering 6(49). https://doi.org/10.3390/jmse6020049.

Breslin, J.P. (1970). 'Theoretical and experimental techniques for practical estimation of propeller-induced vibratory forces'. SNAME Symposium on Ship Vibration, pp 23-40, New York, USA.

Brubakk, E. and Smogeli, H. (1988). QE2 from turbine to diesel - consequences for noise and vibration. In IMAS Conference, The Design and Development of Passenger Ships.

Carlton, J.S. (2007) 'Marine propellers and propulsion', 2nd Ed, Butterworth-Heinemann, Elsevier Ltd.

Cruz, E. Lloyd, T., Bosschers, J., Lafeber, F.H., Vinagre, P. , and Vaz, G., (2021). 'Study on inventory of existing policy, research and impacts of continuous underwater noise in Europe.' EMSA report EMSA/NEG/21/2020. WavEC Offshore Renewables and Maritime Research Institute Netherlands.

Duarte, C. M., Chapuis, L., Collin, S. P., Costa, D. P., Eguiluz, V., Erbe, C., Halpern, B. S., Havlik, M. N., Gordon, T. A. C., Merchant, N. D., Meekan, M., Miksis-Olds, J. L., Parsons, M., Predragovic, M., Radford, A. N., Radford, C. A., Simpson, S. D., Slabbekoorn, H., Staaterman, E., Opzeeland, I.C., Van Winderen, J., Zhang, X. and Juanes, F. (2021). The soundscape of the anthropocene ocean. Science, 371(6529). https://doi.org/10.1126/science.aba4658.

Fréchou, D., Dugué, C., Briançon-Marjollet, L., Fournier, P., Darquier, M., Descotte, L., and Merle, L. (2000). 'Marine propulsor noise investigations in the hydroacoustic water tunnel GTH'. In 23rd Symposium on Naval Hydrodynamics, Val-de-Reuil, France.

Friesch, J. (1998). 'Correlation investigations for higher order pressure fluctuations and noise for ship propellers'. Third International Symposium on Cavitation, Grenoble, France.

Ge, M., Svennberg, U., and Bensow, R. E. (2020). 'Investigation on RANS prediction of propeller induced pressure pulses and sheet-tip cavitation interactions in behind hull condition'. Ocean Engineering, 2020, 209: 107503.

Hämäläinen, R., Lönnberg, B., Aren, P., and Petterson, G. (2005). 'Highest comfort class design for M/S Color Fantasy, the world's largest ever cruise-liner with a car-deck'. In 1st International Ship Noise and Vibration Conference, London, UK.

Johannsen, C., vanWijngaarden, E., Lücke, T., Streckwall, H., and Bosschers, J. (2012). 'Investigation of hull pressure pulses , making use of two large scale cavitation test facilities'. In 8th International Symposium on Cavitation CAV2012, Singapore.

van der Kooij, J. (1979). 'Experimental determination of propeller-induced hydrodynamic hull forces in the NSMB Depressurised Towing Tank'. Symposium on Propeller Induced Ship Vibration. The Royal Institution of Naval Architects.

Lafeber, F.H., van Wijngaarden, E., and Bosschers, J. (2009). 'Computation of hull-pressure fluctuations due to non-cavitating propellers', First International

Symposium on Marine Propulsors SMP'09, Trondheim, Norway.

Li, D.-Q., Hallander, J. and Johansson, T. (2016) Predicting underwater radiated noise of a full scale ship with model testing and numerical methods. Ocean Engineering, 161, 121-135. https://doi.org/10.1016/j.oceaneng.2018.03.027.

Lidtke, A.K., Lloyd, T., Lafeber, F.H., Bosschers, J., 2022. 'Predicting cavitating propeller noise in off-design conditions using scale-resolving CFD simulations'. Ocean Engineering 254, 111176. https://doi.org/10.1016/j.oceaneng.2022.111176.

MacFarlane, G. G. (1949). 'On the energy-spectrum of an almost periodic succession of pulses', Proc. of the Inst. of Radio Eng., Vol. 37, No. 10, pp. 1139-1142

Miglianti, F., Tani, G., Viviani, M., Cipollini, F., Oneto, L. (2019). 'Data driven models for propeller cavitation noise in model scale'. in: Proceedings of the 6th International Symposium on Marine Propulsors, Rome, Italy.

Raestad, A. E. (1996). 'Tip vortex index - an engineering approach to propeller noise prediction'. The Naval Architect, pages 11–16.

Thomsen, F., Mendes, S., Bertucci, F., Breitzke, M., Ciappi, E., Cresci, A. Debusschere, E., Ducatel, C., Folegot, F., Juretzek, C., Lam, F-P., O' Brien, J., dos Santos, M. E. (2021) 'Addressing underwater noise in Europe: Current state of knowledge and future priorities.' Kellett, P., van den Brand, R., Alexander, B., Muniz Piniella, A., Rodriguez Perez, A., van Elslander, J., Heymans, J. J. [Eds.] Future Science Brief 7 of the European Marine Board, Ostend, Belgium. http://dx.doi.org/10.5281/zenodo.5534224.

Vaz, G., Bosschers, J. (2006). 'Modeling three dimensional sheet cavitation on marine propellers using a boundary element method'. Proceedings of the 6th International Symposium on Cavitation, Wageningen, the Netherlands.

Vaz, G., Hally, D., Huuva, T., Bulten, N., Muller, P., Becchi, P., Herrer, J.L.R., Whitworth, S., Mace, R., Korsstrom, A. (2015) Cavitating flow calculations for the E779A propeller in open water and behind conditions: code comparison and solution validation, in: Proceedings of the 4th International Symposium on Marine Propulsors, Austin, USA. pp. 330–345.

van Wijngaarden, H. C. J. (2011). 'Prediction of Propeller-Induced Hull-Pressure Fluctuations'. PhD thesis, Delft University of Technology, the Netherlands.